1987

NASA/ASEE SUMMER FACULTY FELLOWSHIP PROGRAM

MARSHALL SPACE FLIGHT CENTER

INFRARED EMISSION AND TIDAL INTERACTIONS OF SPIRAL GALAXIES

Prepared by:	Gene G. Byrd,Ph.D.
Academic Rank:	Professor of Astronomy
University and Department:	University of Alabama Physics and Astronomy
NASA/MSFC:	
Laboratory:	Space Sciences
Division:	Astrophysics
Branch:	X-Ray Astronomy
MSFC Colleague:	Martin Weisskopf
Date:	August 15, 1987
Contract No.:	The University of Alabama in Huntsville NGT-01-008-021

INFRARED EMISSION AND TIDAL INTERACTIONS OF SPIRAL GALAXIES

by

Gene G. Byrd
Professor of Astronomy
University of Alabama
Tuscaloosa, Alabama

ABSTRACT

We use computer simulations of tidal interactions of spiral galaxies to attempt to understand recent discoveries about infrared(IR) emitting galaxies by Telesco (MSFC), Wolstencroft and Done(Royal Observatory, Edinburgh). We find that the stronger the tidal perturbation by a companion the more disk gas clouds are thrown into nucleus crossing orbits and the greater the velocity jumps crossing spiral arms. Both these tidally created characteristics would create more IR emission by high speed cloud collisions and more IR via effects of recently formed stars. This expectation at greater tidal perturbation matches the observation by Telesco et al. of greater IR emission for spiral galaxies with closer and/or more massive companions. The greater collision velocities found at stronger perturbations in our models will also result in higher dust temperature in the colliding clouds as Telesco et al. also observe. In the IR pairs that Telesco et al. examine, most have only one member, the larger, detected and when both are detected, the larger is always the more luminous. In our simulations and in a simple analytic description of the strong distance depencence of the tidal force, we find that the big galaxy of a pair is more strongly affected than the small in comformity with the results of Telesco et al.

ACKNOWLEDGEMENTS

I would like to express my appreciation to Martin Weisskopf for being my NASA host during this summer. I also appreciate Charles Telesco's conversations on infrared galaxies and sharing his results in advance of publication. Finally, I would like to thank Shigeki Miyaji and Roger Bussard for helpful conversations and computer assistance.

LIST OF FIGURES

1. INTRODUCTION

In order to understand the problem, method, and conclusions of this project it is necessary to recall some background information about spiral galaxies. Spiral galaxies consist of three main parts: the nuclear bulge, the galactic disk and the halo.

The galactic disk consists of stars, hydrogen gas, and dust with the first most important in terms of mass etc. The galactic disk is about 100,000 light years or 30,000 parsecs (30 kpc) across. The material in the galactic disk travels in near circular orbits around its center at 200-250 km/s. The surface density of stars and to a greater degree gas and dust are enhanced in the spiral arms. These arms (usually two) spiral outward from the nucleus in the disk.

The nuclear bulge consists of a concentrated swarm of stars in much more random orbits than the disk material. In the very center of the nuclear bulge is a 1/2 to 1 kpc nuclear disk composed of denser gas in circular orbits around what may be a massive black hole.

The halo is a mysterious component which is as large or larger than the glactic disk. The halo is roughly spherical and contains globular clusters of stars, solitary stars and mysterious undetected dark matter in random tilted orbits. The halo is thought to be roughly equal in mass to the galactic disk although there is considerable disagreement about this.

Most of the mass of the gas in the galactic disk interior to the sun's orbital radius is in molecular hydrogen clouds($\sim 5 \times 10^9$ solar masses). Beyond the sun's orbital radius the hydrogen is primarily atomic but still in clouds. The molecular cloud surface density peaks at 6 kpc from the center with a minimum near the nucleus then another maximum at the center in the nuclear disk (see review by Mihalis and Binney 1981). The gaseous disk is very thin, about 120 pc. Most of the clouds are scattered evenly over the disk in angle. These typical clouds are around 10^5

solar masses and about 20 pc in size. They are very cold, about 2 degrees Kelvin, probably because massive blue stars are not forming in them (Elmegreen 1986). The velocity dispersion among the clouds is a few km/s, much smaller than the disk stellar velocity dispersion.

In contrast, another population of clouds, those with warm cores (about 11 degrees Kelvin) are concentrated in the spiral arms. These clouds are greatly outnumbered by the cold clouds. Formation of groups of O/B stars evidently warms these clouds. These clouds are mostly aggregated in complexes of about a million solar masses (Soloman and Sanders 1986). The formation of these complexes is apparently the result of inelastic encounters among the clouds when they are crowded together in the stellar spiral arms of the disk (Kwan and Valdes 1983, Tomiska 1984). It may be that star formation and gravitational tides upon leaving the spiral arms break up these complexes. They are not found outside the arms and the stellar associations in them are only 10 to 20 million years old, the time to cross an arm.

2. OBJECTIVES

This project will involve infrared(IR) emission by spiral galaxies. This is primarily from heated dust within the gas clouds. the dust can be heated by visual radiation from luminous newly formed stars. The thick dust clouds around such stars do not let the visible out well in contrast to the IR which passes out easily. Another mechanism to generate IR which is more direct is the collision of clouds. If their relative velocity is great enough (greater than 50 km/s), dissociation and ionization of the hydrogen will occur at the collision interface. The resulting visual radiation from the hydrogen will be absorbed and then re-emitted by the dust as IR radiation (Harwit et al. 1987).

My project this summer is related to recent work by C. Telesco (MSFC),R.D.Wolstencroft and C.Done (Royal Observatory, Edinburgh). Telesco et al. (1987) used IRAS data and a sample of interacting pairs of galaxies compiled by Arp and Madore (1987). Telesco et al. studied the emission at 60 and 100 micrometers, defining the parameter R to be the ratio of the 60 to the 100 micrometer fluxes. If

R is larger than 0.5 the galaxy is defined to be "hot", smaller "cool". An R of 0.5 is roughly 60 degrees Kelvin which is hot compared to the 5 degrees typical of molecular clouds in our galaxy.

Telesco et al. measured the angular sizes of pair members and their separations of European Southern Observatory Sky Survey photographs. They could estimate masses of the pair members from the empirical relationship that mass is proportional to size $^{1.5}$. They then could estimate a tidal perturbation perameter equal to the perturber mass (in terms of the galaxy mass) divided by the distance of of the perturber cubed (in terms of the galaxy radius).

Telesco et al. found: (a) a correlation between temperature R and the degree of tidal perturbation in IR emitting pairs. Also stronger tidal perturbation goes with greater IR energy output, (b) a rule that when only one member of a pair was detectable it was the larger member. If both were detectable, the larger was more luminous.

During this summer, I used computer simulations to try to better understand the reasons for (a) and (b) above. I was also interested in the mechanism and location of the IR emission i.e. is it via collisions of clouds and/or via star formation?

3. THE COMPUTER PROGRAM

Our principal tool is a two-dimensional polar coordinate FFT n-body program by Miller (1976, 1978). the coordinate grid of this program is well suited for study of disk galaxies providing high spatial resolution where it is most needed, near the center (see Figure 1). We use about 60,000 particles to simulate the disk of the spiral galaxy. Each part of the disk acts gravitationally on all other parts of the disk, i.e. the disk is self-gravitating.

Major parameters of our study were the ratio of the halo mass to the disk mass and the velocity dispersion in the galaxy's disk. We expect the halo to have a high velocity dispersion and, therefore, to be much more stable than the "cooler" disk. Accordingly, we followed Miller (1978)

and considered the halo to be inert. Increasing the halo to disk mass helps stabilize the disk, as does increasing the disk velocity dispersion (Toomre 1964). The spatial softening due the program grid and a constant in the gravitational potential formula assumed have the same stabilizing effect as the velocity dispersion (Miller 1971,1974,1978). Using Miller (1978), the spatial softening of our model disk is equivalent to a velocity dispersion of about 1.5 times that sufficient to stabilize it against small axisymmetric perturbations. This assumed dispersion is about that seen in stellar disks of spiral galaxies. We thus used only this softening to simulate the stellar disk velocity dispersion. The-halo-to-disk mass ratio is taken to be one.

4. PREVIOUS USE OF THE PROGRAM

This program has been used to study the onset of global instability and subsequent changes in a disk composed primarily of stars (Miller 1978). The unmodified program has also been used to study the onset of global instabilities in a gaseous disk (Cassen, Smith, Miller 1981). We have modified the program to simulate a finite rather than the infinite disk studied by Miller and co-workers. We also modified the program to simulate the tidal effect of a companion on the disk of a spiral galaxy. We also used this version to study the capture and orbital decay of satellites of disk galaxies (Byrd, Saarinen, Valtonen 1986) and the creation of spiral arm spurs by large gas complexes in galaxy disks (Byrd,Smith, Miller 1984).

The most recent use of this program and most relevant use to the present project is simulate the tidal triggering of Seyfert galaxy activity by companions (Byrd, Sundelius and Valtonen 1986; Byrd,Valtonen, Sundelius, and Valtaoja 1987). In this investigation, the companions may trigger inflows of disk material into the nucleus to fuel activity there. We have used the program to simulate the tidal action of the companion on the disk of a spiral galaxy and show that the tidal strengths at which large inflows appear match those of the observed companions of Seyferts.

Our fundamental method for estimating gas cloud flow into the nuclear regions was very crude. We simply counted how many of the 60,000 particles/step were thrown into orbits crossing the 1 kpc nuclear region. This fraction times the assumed fraction of the disk in gas (0.10) times the assumed disk mass (1×10^{11} solar masses, 20 kpc) equals the rate gas entered the nuclear regions. From observations, the rate was required to be greater than or equal to 0.5 solar masses/yr. This gas, once thrown into such orbits, will collide with other gas clouds or the nuclear disk to flow into the "engine". Small scale accretion processes near the central black hole were beyond the scope of our investigation.

According to our simple previous calculations, smaller tidal perturbations result in weaker inflows in our model. Tidal perturbation levels (as previously defined) of 0.01 to 0.1 (depending on the mass of the halo) are necessary to produce the required inflows. Dahari (1984) finds observationally that most spiral galaxies perturbed at these levels or greater are Seyferts.

5. AN EXAMPLE OF A PROGRAM RUN AND OUTPUT

In the example shown in Figure 2, we see the shapes generated during an encounter of a galaxy with a perturber 0.22 of the galaxy's mass which approaches in a zero energy orbit to within two disk radii of the galaxy. The halo to disk mass ratio is assumed to be one. The disk has 60,000 particles.

The time covered is about three revolutions of the disk edge. Circular orbit velocity in the disk is 208 km/s. The darkness in the figure indicates particle surface density. The unit of length in the program is equal to about one kpc. The total mass of the galaxy is 2×10^{11} solar masses. The disk of the galaxy is 20 units in radius, about 1/3 of the grid radius. The perturber enters the grid on the right at 0 degrees and swings by in a counter clockwise sense, the same as the disk rotation and the measurement of the angular position of the perturber.

Figure 3 shows a display of the number of particles in each of the bins in our example run. The underlines show the density peaks along a spiral arm created by the tidal

action. The horizontal bin rows are by azimuth every 10 degrees starting zero at the top. The 24 columns are radial with the edge of the grid at the right.

Figure 4 shows the average radial velocities of the particles in the bins (zero for bins with no particles or with zero rv). For an undisturbed disk, all values should be zero since the particles are initially in circular orbits. However, there are inward (-) and outward (+) velocities as a result of the tidal perturbation. Divide the values by three to get velocities in km/s. We see the velocity differences in Figure 4 are not large compared to the original circular orbital velocity of 208 km/s.

6. EXPLAINING RESULTS FOUND BY TELESCO ET AL.

We will use these displays of the results of the above and other computer runs to explain the reasons found by Telesco et al. in their observations. First, let us consider the first two correlations for IR emitting pairs of interacting galaxies. As we noted in our earlier work on Seyfert galaxies, stronger tidal perturbation results in greater inflow into the nuclear regions. Considering our previous "example" run, we find that it causes no inflow to the 1 kpc nuclear regions. Note how the radial velocities in the bins near the center are zero in Figure 4.

Now consider a stronger run with the mass increased to 0.44 the galaxy's mass and the close approach distance 0.75 of its value in the other run. This reduction results in an increase in tidal perturbation to 5x the previous value. Figure 5 shows the shape of the disturbed galaxy 900 time steps(900 million years) after the perturber entered the grid. Counts within the program show that at least 1/3 of the disk particles are thrown into orbits crossing the inner 1 kpc, much more than in the weaker perturber run.

Figure 6 shows the radial velocities in the different bins for this stronger run. Surprisingly,the radial velocities inward near the nucleus are only around 20 km/s. The high surface densities near the center help result in the large total inflow. However, the IR emission from the nucleus (due to the inflow) would probably be created later in the nuclear disk (via star formation etc.), rather than from the velocity of collision with the disk.

However, the stronger run shows interesting events in the disk. The radial velocity deviations are about five times those in the weaker run. Inward and outward flows of about 100 km/s are seen. In particular, large inward and outward velocities are found in outer and inner bins respectively at the same azimuth. It seems that in the outer disk collisions at speeds sufficient to excite IR directly will occur. Of course, after these collisions one would expect massive stars to quickly form and produce indirect IR emission. So IR emission should be seen from the disk of the galaxy as well as the nuclear regions.

The correlation between temperature and tidal perturbation is explained also. Greater velocity differences resulting from stronger perturbation encounters result in more energy release in collisions, greater grain temperatures and hotter IR temperature emission.

The final pattern that Telesco et al. found was that most interacting pairs detectable in IR had only one detectable member. When both were detected, the larger was always more IR luminous.

The strong variation of tidal force with distance (inverse cubed) is probably the major factor in the large versus small pattern. Consider the following example of a massive primary and a companion galaxy one-half the mass of the primary. They are two disk radii of the primary apart. The nearer edge of the primary to the secondary has a tidal perturbation on it eight times that on the primary's center. The far edge has a tidal perturbation only one-third that at the center.

The secondary galaxy is smaller by a factor of $0.5^{1.5}$. The perturbation at the center of the secondary is the same as at the center of the primary. The nearer edge of the secondary is perturbed by a factor of only 1.8 times that at the secondary's center while the far edge factor is 0.6. The difference between the two edges is not so great as for the primary and the near edge is not perturbed nearly so strongly as the near edge of the primary. We thus see that the size of the galaxy relative to the distance of its perturber is very important.

The two computer runs discussed earlier show this effect of size relative to separation. Recall that the encounter distance was decreased by 25% in the second run. The closer encounter result is much more asymmetric with the nearer arm much stronger. The surface density asymmetry between the two main arms in the close encounter is 2/1 in the close encounter but it is only 1.1/1 for the far encounter. The strength of the stronger arm and the arm-interarm contrast is greater for the closer encounter.

We have also done a run of a disk perturbed by a symmetric tidal field to the same level at the center as our close encounter above. Interestingly, the nuclear inflow is much smaller for the symmetric, distant perturber run. Possiby the strong asymmetric arm structure helps promote nuclear inflow after it forms.

The above explains results found by Telesco et al. for small versus large members of a pair. The fact that the more massive galaxy is larger relative to the pair separation than the less massive could be the cause of the emission difference.

7. SUMMARY AND LIMITS OF CONCLUSIONS

We see that the IR emission could come from the disk as well as the nucleus according to our simulations. Increasing the strength of the perturbation should increase the emission and make it occur at a higher temperature. The larger size of the more massive pair member relative to the pair separation causes its emission to be stronger. Also the disk emission should be more asymmetric in the more massive member for the same reason. These patterns match those observed by Telesco et al.

The above conclusions apply to tidally interacting but not colliding spirals or merging galaxies. The conclusions also do not apply to the case where one galaxy tears significant amounts of material from the other. This could be one way for the small galaxy to be more luminous in some cases. Unfortunately, the IRAS data is not good enough to show the morphology of IR emission within the pair members. While some nearby systems show the expected asymmetries, a large enough sample observed sufficiently well will be an important project for the future.

REFERENCES

Arp,H.C. and Madore,B.F. 1987. A Catalogue of Southern Peculiar Galaxies and Associations (David Dunlap Observatory: Ontario, Canada) in press.

Byrd, G. G., Smith, B. F., and Miller, R. H. 1984, Astrophys.J. 286, 62.

Byrd, G.G., Saarinen, S.,Valtonen, M.J. 1986 Monthly Notices Roy. Astron. Soc. 220, 619.

Byrd, G. G., Valtonen, M.J., Sundelius, B. and Valtaoja, L. 1986 Astron. Astrophys. 166,75.

Byrd, G.G., Sundelius, B., and Valtonen,M. 1987 Astron. Astrophys. 171, 16.

Cassen,P.M.,Smith,B.F., Miller, R.H., and Reynolds, R.T. 1981, Icarus 48, 377.

Dahari, O. 1984, Astron.J. 89, 966.

Elmegreen,B.G. 1986, "Molecular Clouds and Star Formation: An Overview" in Protostars and Planets II, eds. D.C. Black and M.S. Matthews, Univ. of Arizona Press, Tucson, Arizona, p. 33.

Harwitt, M.,Houck,J.P.,Soifer,B.T. and Palumbo,G.G.C. 1987 Astrophys. J. 315, 28.

Kwan,T. and Valdes,F. 1983 Astrophys. J., 271, 604.

Mihalas, D. and Binney, J. 1981, Galactic Astronomy-Structure and Kinematics (W.H. Freeman, San Francisco) p.545-565.

Miller, R.H. 1971, Astrophys. and Space Science 14, 73.

Miller, R.H. 1974, Astrophys. J. 190, 539.

Miller, R.H. 1978, Astrophys. J. 224, 32.

Sanders,D.B.,Solomon,P.M. and Scoville, N.Z. 1984, Astrophys. J. 276. 182.

Solomon,P.M and Sanders,D.B. 1986,"Star Formation in a Galactic Context: The Location and Properties of Molecular Clouds," in Protostars and Planets II, ed. D.C.Black and M. S. Matthews, Univ. of Arizona Press, Tucson, Arizona, p. 59.

Telesco, C.M.,Wolstencroft,R.D. and Done, C. 1987 (private communication).

Tomiska,K. 1984, P.A.S.J. 36,457.

Toomre, A. 1964, Astrophys. J. 139, 1217.

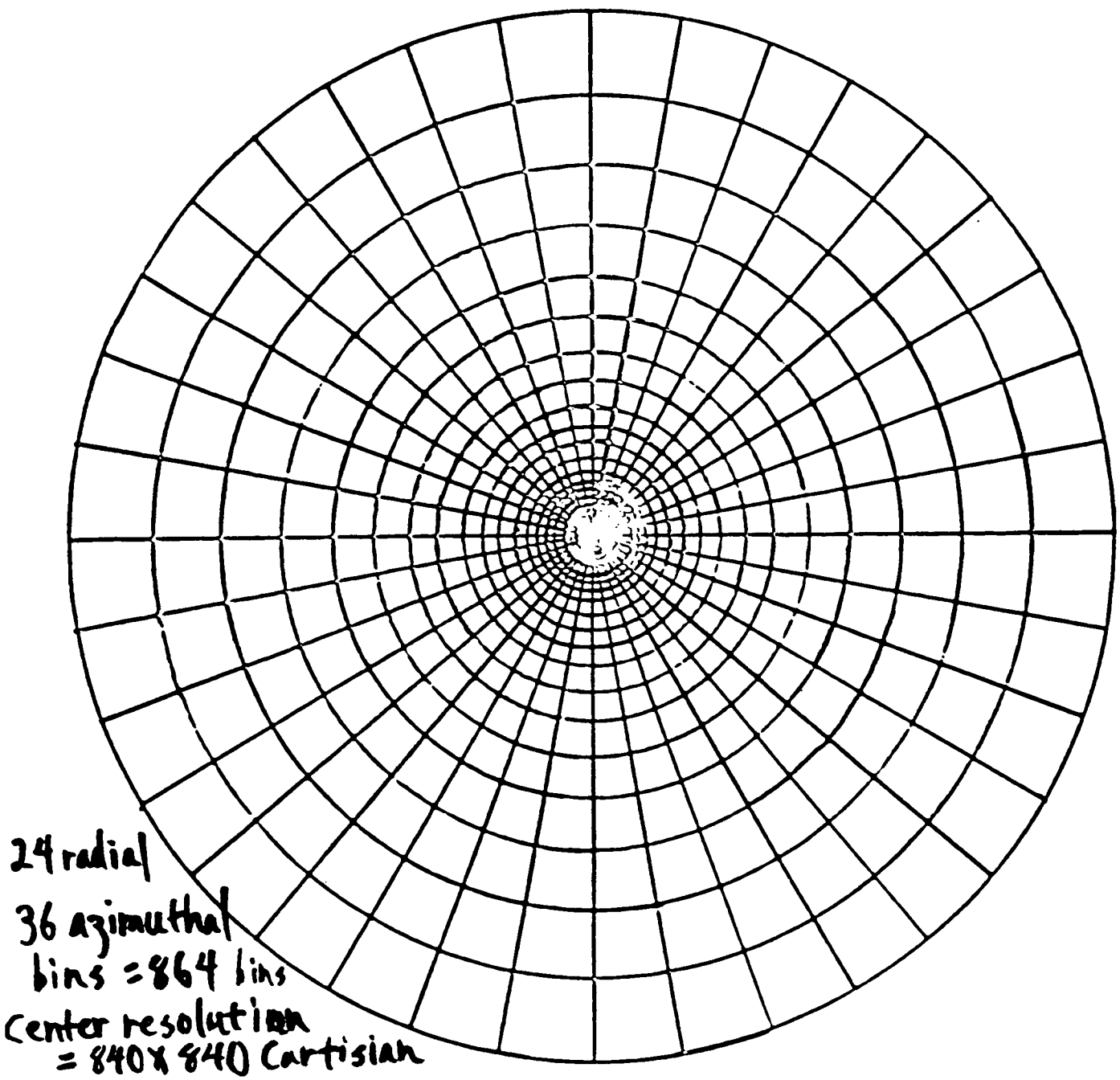

Figure 1-Grid used in computer program.

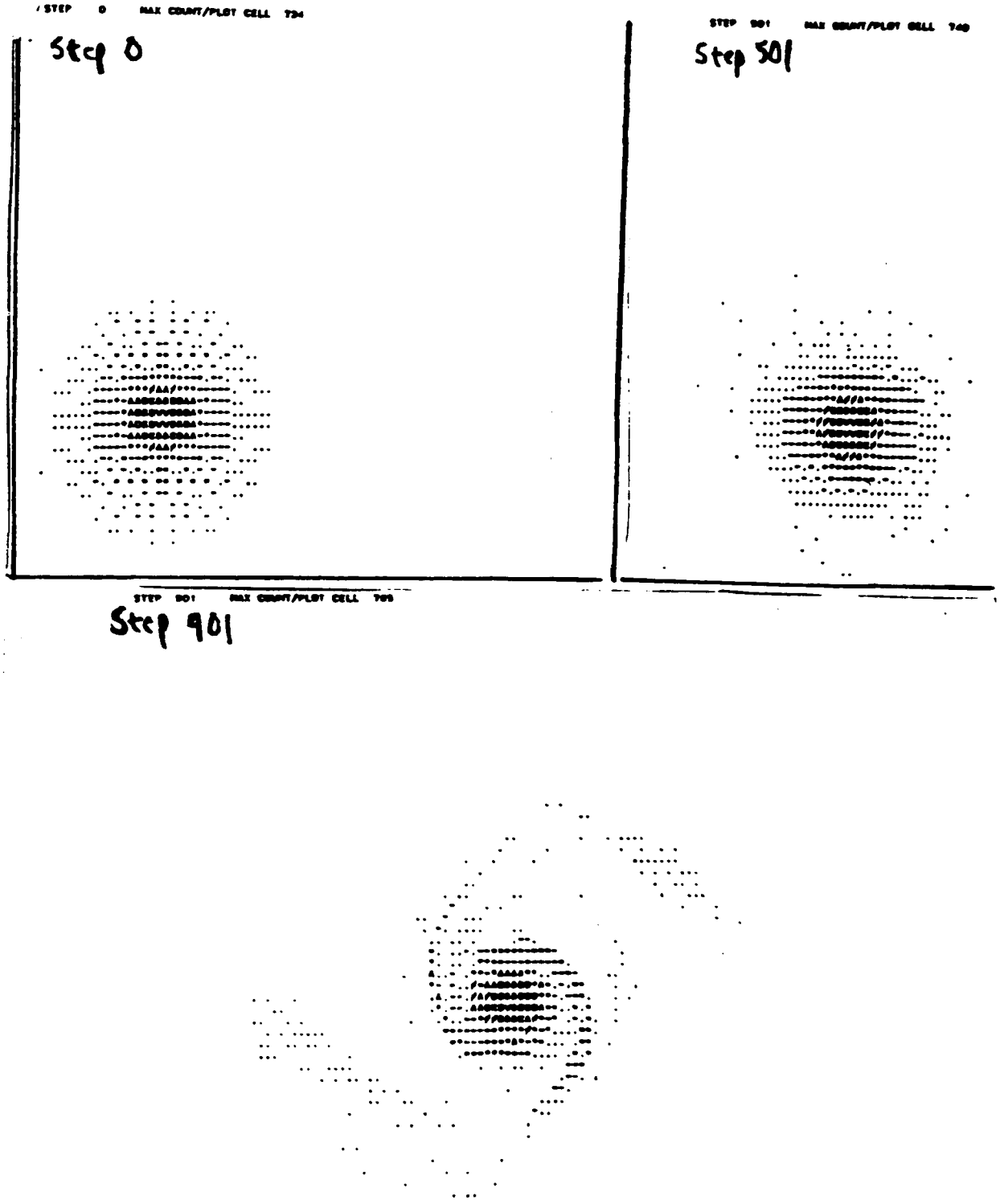

Figure 2-Example of spiral arm generation during simulation

center radial bins edge

1	2	3	4	5	6	7	8	9	10	11	12	13	14	15	16	17	18	19	20	21	22	23	24
11.0	27.0	32.0	38.0	44.0	57.0	44.0	86.0	87.0	107.0	99.0	138.0	91.0	184.0	289.0	76.0	3.0	3.0	0.0	0.0	0.0	0.0	0.0	0.0
11.0	27.0	32.0	38.0	45.0	51.0	50.0	90.0	76.0	98.0	104.0	89.0	151.0	211.0	228.0	92.0	3.0	4.0	0.0	0.0	0.0	0.0	0.0	0.0
11.0	27.0	32.0	38.0	46.0	49.0	53.0	82.0	75.0	81.0	158.0	46.0	126.0	266.0	154.0	106.0	6.0	2.0	0.0	0.0	1.0	0.0	0.0	0.0
11.0	27.0	32.0	38.0	46.0	45.0	53.0	83.0	75.0	89.0	155.0	54.0	147.0	250.0	76.0	85.0	15.0	5.0	0.0	4.0	7.0	0.0	0.0	0.0
11.0	27.0	32.0	38.0	47.0	46.0	56.0	89.0	79.0	94.0	115.0	58.0	135.0	220.0	83.0	118.0	33.0	5.0	0.0	3.0	15.0	0.0	0.0	0.0
11.0	27.0	32.0	38.0	45.0	49.0	61.0	88.0	89.0	124.0	87.0	79.0	147.0	242.0	87.0	100.0	71.0	9.0	0.0	12.0	12.0	0.0	0.0	0.0
11.0	27.0	32.0	38.0	42.0	54.0	61.0	91.0	83.0	102.0	76.0	100.0	135.0	220.0	48.0	74.0	108.0	60.0	0.0	10.0	9.0	0.0	0.0	0.0
11.0	27.0	32.0	38.0	43.0	54.0	80.0	72.0	74.0	104.0	74.0	134.0	136.0	201.0	73.0	48.0	79.0	74.0	2.0	46.0	7.0	0.0	0.0	0.0
11.0	27.0	32.0	38.0	44.0	48.0	88.0	61.0	73.0	109.0	53.0	137.0	203.0	146.0	124.0	90.0	188.0	105.0	45.0	255.0	2.0	0.0	0.0	0.0
11.0	27.0	32.0	38.0	47.0	52.0	81.0	61.0	67.0	133.0	55.0	135.0	206.0	80.0	120.0	118.0	197.0	28.0	328.0	85.0	0.0	0.0	0.0	0.0
11.0	27.0	32.0	38.0	47.0	54.0	64.0	64.0	66.0	115.0	63.0	126.0	223.0	52.0	68.0	122.0	184.0	123.0	181.0	0.0	0.0	0.0	0.0	0.0
11.0	27.0	32.0	37.0	45.0	70.0	54.0	57.0	61.0	120.0	56.0	146.0	207.0	72.0	102.0	233.0	89.0	262.0	6.0	0.0	0.0	0.0	0.0	0.0
11.0	27.0	32.0	37.0	42.0	65.0	48.0	50.0	74.0	105.0	58.0	146.0	184.0	127.0	159.0	194.0	252.0	37.0	0.0	0.0	0.0	0.0	0.0	0.0
11.0	27.0	32.0	37.0	46.0	63.0	42.0	52.0	75.0	105.0	65.0	217.0	105.0	139.0	159.0	128.0	280.0	3.0	0.0	0.0	0.0	0.0	0.0	0.0
11.0	27.0	32.0	38.0	48.0	68.0	37.0	57.0	75.0	101.0	75.0	211.0	60.0	119.0	176.0	210.0	110.0	4.0	0.0	0.0	0.0	0.0	0.0	0.0
11.0	27.0	32.0	38.0	53.0	56.0	39.0	68.0	80.0	116.0	100.0	185.0	74.0	120.0	131.0	451.0	38.0	9.0	0.0	0.0	0.0	0.0	0.0	0.0
11.0	27.0	32.0	39.0	53.0	47.0	50.0	70.0	72.0	108.0	128.0	143.0	97.0	123.0	338.0	229.0	15.0	0.0	0.0	0.0	0.0	0.0	0.0	0.0
11.0	27.0	32.0	40.0	53.0	39.0	49.0	81.0	87.0	101.0	187.0	62.0	103.0	130.0	428.0	64.0	11.0	0.0	0.0	0.0	0.0	0.0	0.0	0.0
11.0	27.0	31.0	40.0	51.0	35.0	57.0	72.0	72.0	103.0	171.0	77.0	126.0	170.0	360.0	49.0	5.0	0.0	0.0	0.0	4.0	4.0	0.0	0.0
11.0	27.0	32.0	40.0	44.0	41.0	66.0	68.0	95.0	86.0	153.0	63.0	134.0	233.0	210.0	41.0	5.0	0.0	0.0	3.0	14.0	9.0	0.0	0.0
11.0	27.0	32.0	40.0	43.0	48.0	58.0	71.0	111.0	86.0	126.0	121.0	110.0	296.0	121.0	65.0	13.0	0.0	2.0	8.0	32.0	3.0	0.0	0.0
11.0	27.0	32.0	40.0	47.0	57.0	58.0	62.0	104.0	128.0	52.0	123.0	136.0	299.0	80.0	70.0	8.0	0.0	4.0	11.0	0.0	0.0	0.0	0.0
10.0	27.0	32.0	40.0	45.0	60.0	64.0	67.0	96.0	111.0	43.0	107.0	152.0	295.0	74.0	94.0	12.0	0.0	7.0	0.0	7.0	0.0	0.0	0.0
11.0	27.0	32.0	38.0	44.0	59.0	61.0	76.0	90.0	101.0	42.0	122.0	145.0	278.0	58.0	125.0	25.0	1.0	2.0	10.0	25.0	0.0	0.0	0.0
11.0	27.0	33.0	38.0	46.0	58.0	59.0	82.0	67.0	80.0	40.0	150.0	137.0	244.0	78.0	137.0	22.0	18.0	9.0	45.0	9.0	0.0	0.0	0.0
12.0	27.0	32.0	38.0	45.0	55.0	64.0	98.0	50.0	105.0	49.0	177.0	228.0	167.0	95.0	139.0	53.0	77.0	61.0	56.0	0.0	0.0	0.0	0.0
11.0	27.0	32.0	38.0	47.0	52.0	70.0	74.0	49.0	73.0	67.0	173.0	301.0	80.0	93.0	106.0	99.0	156.0	196.0	84.0	0.0	0.0	0.0	0.0
11.0	27.0	32.0	38.0	44.0	53.0	68.0	82.0	45.0	96.0	147.0	144.0	199.0	68.0	82.0	105.0	130.0	219.0	275.0	0.0	0.0	0.0	0.0	0.0
11.0	27.0	32.0	38.0	45.0	53.0	68.0	78.0	40.0	99.0	149.0	109.0	175.0	77.0	58.0	115.0	246.0	207.0	5.0	0.0	0.0	0.0	0.0	0.0
11.0	27.0	32.0	38.0	44.0	56.0	71.0	63.0	49.0	127.0	138.0	115.0	193.0	79.0	64.0	100.0	315.0	137.0	0.0	0.0	0.0	0.0	0.0	0.0
11.0	27.0	32.0	38.0	44.0	53.0	71.0	63.0	62.0	102.0	139.0	140.0	146.0	94.0	61.0	226.0	260.0	28.0	0.0	0.0	0.0	0.0	0.0	0.0
11.0	27.0	32.0	38.0	46.0	54.0	69.0	57.0	76.0	115.0	126.0	130.0	153.0	97.0	80.0	345.0	137.0	0.0	0.0	0.0	0.0	0.0	0.0	0.0
11.0	27.0	32.0	38.0	45.0	55.0	59.0	64.0	89.0	90.0	104.0	141.0	93.0	77.0	164.0	409.0	38.0	0.0	0.0	0.0	0.0	0.0	0.0	0.0
11.0	27.0	32.0	38.0	46.0	56.0	56.0	61.0	112.0	106.0	90.0	185.0	77.0	98.0	273.0	349.0	9.0	0.0	0.0	0.0	0.0	0.0	0.0	0.0
11.0	27.0	32.0	38.0	45.0	57.0	49.0	60.0	106.0	107.0	94.0	182.0	51.0	119.0	279.0	262.0	17.0	0.0	0.0	0.0	0.0	0.0	0.0	0.0
11.0	27.0	32.0	38.0	44.0	60.0	53.0	62.0	112.0	117.0	94.0	134.0	84.0	182.0	317.0	118.0	3.0	0.0	0.0	0.0	0.0	0.0	0.0	0.0

Figure 3-Number of particles in grid bins at step 901,Fig.2.

0	0	0	0	0	3	36	5	-12	-28	-5	-6	70	10	-95	15	143	196	0	0	0	0	0	0
0	0	0	0	0	7	34	-10	-14	-26	-12	3	26	-27	-96	43	146	178	0	0	0	0	0	0
0	0	0	0	0	13	29	-16	-11	-14	-20	25	0	-70	-71	77	150	154	0	0	115	0	0	0
0	0	0	0	0	17	23	-22	-7	-5	-24	22	-5	-79	-15	93	156	155	0	83	110	0	0	0
0	0	0	0	1	21	14	-25	-8	-8	-27	12	-12	-74	8	106	154	129	0	93	103	0	0	0
0	0	0	0	3	22	3	-31	-10	-13	-18	6	-11	-55	32	109	141	119	0	109	105	0	0	0
0	0	0	0	3	16	-10	-34	-8	-15	0	12	-19	-44	43	103	112	38	0	144	110	0	0	0
0	0	0	0	3	7	-29	-27	-2	-4	7	18	-24	-24	66	108	152	33	44	139	168	0	0	0
0	0	0	0	3	1	-36	-15	6	0	13	14	-39	6	83	116	121	64	87	111	144	0	0	0
0	0	0	0	2	-6	-39	-3	14	1	25	15	-42	27	79	123	68	43	57	110	0	0	0	0
0	0	0	0	0	-17	-37	5	19	3	33	21	-30	39	87	114	25	-7	8	0	0	0	0	0
0	0	0	0	-1	-29	-21	16	19	7	47	12	-18	65	107	73	2	-63	-52	0	0	0	0	0
0	0	0	0	-4	-33	-5	25	20	15	54	5	-14	77	86	39	-79	-85	0	0	0	0	0	0
0	0	0	0	-7	-29	11	35	22	25	57	-5	-9	87	48	24	-103	4	0	0	0	0	0	0
0	0	0	0	-10	-19	23	41	20	31	50	-16	27	77	38	-80	-95	5	0	0	0	0	0	0
0	0	0	0	-12	-5	34	41	24	31	34	-24	47	73	40	-69	-97	9	0	0	0	0	0	0
0	0	0	-1	-10	12	45	32	21	21	5	-18	62	62	-57	-91	-77	0	0	0	0	0	0	0
0	0	0	0	-6	24	46	24	15	8	-21	29	63	53	-78	-90	-47	0	0	0	0	0	0	0
0	0	0	0	0	31	36	16	7	1	-20	33	52	12	-95	-63	-11	0	0	0	-47	47	0	0
0	0	0	0	5	34	23	11	-7	-1	-19	36	37	-51	-62	-9	56	0	0	-121	-9	95	0	0
0	0	0	0	8	30	12	3	-22	-9	-12	37	22	-53	-35	33	64	0	-192	-121	65	110	0	0
0	0	0	0	10	20	0	-7	-35	-27	26	35	13	-58	2	72	100	0	-153	66	0	0	0	0
0	0	0	0	11	10	-3	-17	-40	-25	44	37	16	-55	27	94	107	0	-159	0	102	0	0	0
0	0	0	0	10	4	-4	-28	-41	-13	53	41	23	-47	62	105	119	-183	-113	50	106	0	0	0
0	0	0	0	8	0	-5	-37	-18	0	62	25	28	-32	80	97	160	79	73	63	130	0	0	0
0	0	0	0	5	-2	-8	-37	2	28	71	21	-19	-5	81	96	134	111	107	101	0	0	0	0
0	0	0	0	2	-2	-8	-29	23	45	66	15	-52	46	93	104	139	116	62	93	0	0	0	0
0	0	0	0	1	-2	-10	-16	40	57	31	-2	-53	60	106	113	115	53	33	0	0	0	0	0
0	0	0	0	0	-1	-11	-1	52	52	13	-7	-43	78	108	115	67	-38	-12	0	0	0	0	0
0	0	0	0	0	0	-11	13	53	33	-5	-9	-17	92	111	114	-2	-58	0	0	0	0	0	0
0	0	0	0	0	0	-9	25	44	11	-14	-19	-2	99	113	56	-63	-65	0	0	0	0	0	0
0	0	0	0	0	0	-4	36	18	-2	-21	-17	19	105	120	3	-116	0	0	0	0	0	0	0
0	0	0	0	0	0	0	41	0	-4	-22	-12	17	112	84	-39	-121	0	0	0	0	0	0	0
0	0	0	0	0	0	8	41	-12	-9	-9	-11	71	103	31	-89	-42	0	0	0	0	0	0	0
0	0	0	0	0	0	17	39	-16	-15	3	-14	80	83	-25	-94	-8	0	0	0	0	0	0	0
0	0	0	0	0	0	31	26	-13	-23	1	-10	91	33	-85	-28	150	0	0	0	0	0	0	0

Figure 4-Av. radial velocities in grid bins,step 901,Fig.2

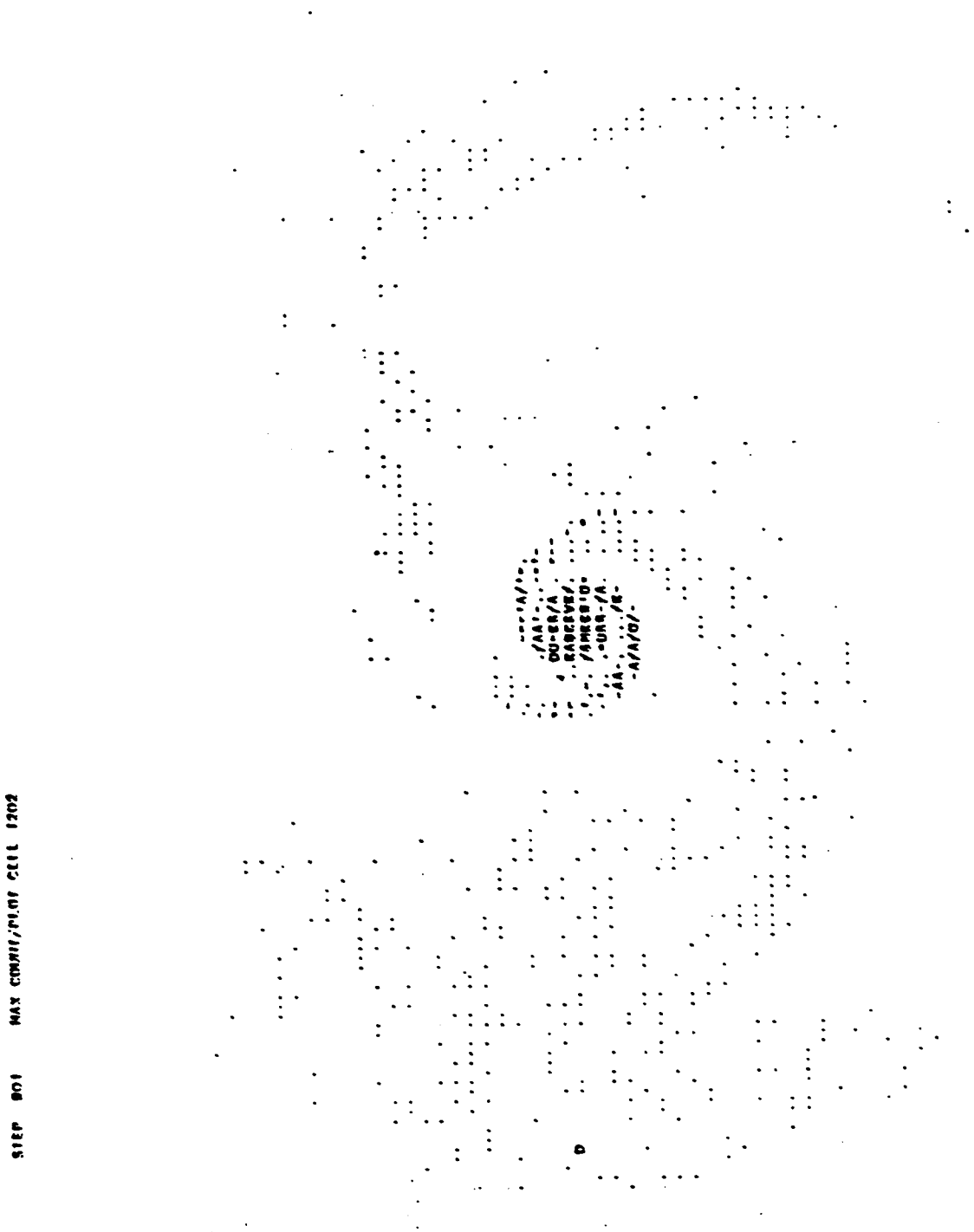

Figure 5-Disturbed disk in closer encounter run than Fig. 2

STEP 900 RAD VEL AV

Divide by 3 to convert to km/s

12	58	-81	-29	199	74	-55	-85	-22	176	222	235	22	-164	-263	30	-236	0	0	0	0	0	244	294
18	51	-76	20	180	13	-90	-7	-44	265	185	158	-47	-204	3	-66	1389	-75	0	0	0	0	250	294
10	42	-78	38	143	-62	-59	-106	88	232	366	89	-142	-74	177	148	-110	-52	0	0	0	0	252	343
21	26	-72	23	50	-83	3	-14	155	288	345	-4	-87	-39	122	248	191	116	-222	-37	119	188	263	375
12	-11	-94	106	3	-68	-33	9	318	311	299	-41	-81	72	74	203	191	134	144	0	106	178	273	343
12	-41	7	106	-6	-77	-21	83	274	328	-41	-126	-98	34	33	-2	91	92	-124	36	101	166	225	0
12	-63	64	120	-39	-26	-41	231	318	323	-217	-136	-51	39	107	-48	79	-13	-71	20	64	129	0	0
15	-51	96	137	0	-95	-59	265	284	-125	-234	-49	-60	4	-77	-89	29	-185	-88	-20	36	0	0	0
-3	-22	112	112	-5	-71	17	263	156	-247	-165	-114	-133	-81	-153	27	-169	-229	-106	-36	0	0	0	0
-1	-14	121	77	-36	-53	87	304	-48	-137	-141	-78	-76	-49	-104	-74	-268	-197	-97	0	0	0	0	0
-2	-13	127	55	-19	-63	271	170	-220	32	-95	-23	-79	-133	-131	-103	-307	-179	-66	0	0	0	0	0
0	7	126	75	-31	-75	333	-31	-105	-72	6	-109	-24	-216	-197	-195	-262	-122	0	0	0	0	0	0
0	18	119	41	-48	-48	349	-9	-14	-62	-26	56	92	-132	-169	-276	-177	-8	0	0	0	-130	-1	0
-11	30	117	38	-83	185	304	-94	-139	-49	176	99	63	-120	-234	-307	-99	23	0	0	0	-61	-5	0
-7	34	120	-19	-42	380	166	-161	-28	-43	186	121	-38	-186	-228	-151	-2	0	-335	-188	-142	-25	30	126
-1	40	134	-44	-25	381	73	-138	-28	-37	205	127	-103	-163	-226	-88	11	38	0	-115	-21	42	126	130
5	41	77	-70	55	361	-133	-64	-70	276	241	150	-106	-149	-272	-46	104	144	-179	-79	75	186	199	221
1	40	24	-80	77	387	-160	-54	-61	328	267	136	-79	-210	-240	8	129	-15	0	-11	149	262	246	255
-8	30	-74	-63	136	311	-114	-14	-43	352	255	201	-191	-230	-16	54	149	211	-180	-109	121	268	399	293
-1	30	-84	-15	183	100	-119	-24	226	522	307	193	-149	-239	88	66	154	224	164	160	0	361	541	205
11	27	-87	8	136	-137	-111	-27	444	501	312	195	-151	-242	100	86	178	214	80	-87	-37	138	225	346
9	8	-91	31	157	-110	-68	-21	369	397	535	182	-174	193	174	105	137	158	198	-122	28	82	297	337
-3	-51	-48	60	133	-153	-110	121	368	380	346	-85	-197	137	132	57	63	127	-27	-109	29	63	0	443
-7	-61	10	77	51	-158	-40	252	355	355	307	-92	-158	199	204	133	71	68	-201	-79	28	103	0	0
0	-60	50	91	-38	-111	46	357	354	342	-42	-157	132	231	232	116	-40	-189	-105	-33	18	0	0	0
0	-51	71	111	-75	-76	31	344	357	291	-149	-132	174	223	246	29	-64	-203	-175	-1	70	0	0	0
5	-45	87	121	-102	-30	-4	339	379	307	-149	-97	170	226	100	19	-201	-190	-80	7	0	0	0	0
-6	-37	100	108	-97	-42	231	304	350	96	-158	5	199	189	55	16	-285	-156	-63	64	0	0	0	0
-14	-27	104	87	-84	-18	282	312	290	-55	-170	95	213	207	-53	42	-200	-141	6	45	0	0	0	0
-14	-8	114	3	-92	-67	308	306	335	-204	-83	158	145	129	-12	-88	-192	-76	11	0	0	0	0	0
-19	9	99	-37	-89	105	331	311	-27	-171	41	187	125	29	-14	-206	-173	-69	-2	0	0	0	0	0
-12	34	93	-67	-68	319	331	328	-215	-25	92	193	166	-67	21	-199	-116	-92	0	0	0	0	0	0
-15	63	84	-85	-40	331	332	-48	-162	0	240	217	68	-39	24	-192	-166	-94	348	264	0	0	0	0
-11	62	74	-111	67	329	239	-211	-65	40	257	187	95	-41	-81	-211	-182	0	0	230	0	0	0	0
1	67	56	-109	137	289	27	-156	35	32	269	240	14	-40	-190	-254	0	269	1068	0	0	0	0	882
8	68	-55	-100	169	218	-149	-110	-19	149	279	325	-6	-12	-247	632	0	1790	0	0	0	0	972	385

Figure 6-Av. velocity of particles in grid bins, closer encounter run of Figure 5.